Smearlets: A Biorthogonal Gaussian Framework for Inverting Space-Variant Point Spread Functions

Zachary Mullaghy*

October 1, 2025

Abstract

We introduce *Smearlets*: finite, multiscale Gaussian families rendered biorthogonal via Gram matrix inversion. This constructive framework is designed for the analysis and inversion of problems involving space-variant blur. The resulting reproducing kernel, $K_N(x, y) = \boldsymbol{u}(x)^\top \boldsymbol{G}^{-1}\boldsymbol{u}(y)$, acts as a finite-rank, space-variant point spread function (PSF) and a delta-reconstruction operator. We formalize the system's response to a Dirac delta by defining its *spectral fingerprint*, $\boldsymbol{v}(x_0) = \boldsymbol{G}^{-1}\boldsymbol{u}(x_0)$, and prove modewise, pointwise, and distributional convergence for delta sequences. We interpret the framework as a measurement theory for the "scale content" of a signal, with the fingerprint acting as a "de Broglie spectrum." Numerical experiments validate the theory, visualizing the basis and demonstrating its application to a 1D space-variant deconvolution problem, where it provides a stable and accurate reconstruction along failure modes of known methodologies.

1 Introduction

The accurate modeling and inversion of blur are fundamental challenges in imaging science. In many high-performance imaging systems, such as positron emission tomography (PET), computed tomography (CT), and wide-field microscopy, the system's point spread function (PSF) is not spatially invariant; its shape, orientation, and scale can vary significantly across the field of view [8, 9]. This space-variant blur complicates reconstruction and deconvolution, as standard Fourier-based methods, which assume a stationary convolution, produce severe artifacts.

While wavelet and shearlet transforms offer powerful multiscale analysis, their fixed atom shapes can be suboptimal for features that are intrinsically smooth or Gaussian, like many PSFs. An alternative is to use dictionaries of Gaussian atoms, such as in Gaussian Mixture Models (GMMs), but these often result in overcomplete, non-orthogonal representations where signal analysis (i.e., finding stable coefficients) is a non-trivial inverse problem in itself.

This paper introduces a constructive and computationally straightforward framework we call *Smearlets*, designed specifically for the analysis and inversion of space-variant blur. We begin with a simple, finite family of multiscale Gaussians and render them biorthogonal through Gram matrix inversion. This process generates a stable dual basis perfectly adapted for signal analysis, bridging the gap between the analytic simplicity of Gaussian atoms and the rigorous stability of biorthogonal systems. This approach provides a direct method to construct a finite-rank, space-variant PSF model from first principles.

Contributions. The primary contributions of this work are threefold:

(i) We define the Smearlet system and derive its associated reproducing kernel, $K_N(x, y)$, showing its natural interpretation as a finite-rank, space-variant PSF.

*Independent Researcher. Email: mullaghymath@gmail.com

(ii) We formalize the system's interaction with distributions by defining the *spectral fingerprint* of the Dirac delta. We prove a convergence theorem detailing the modewise, pointwise, and distributional convergence for delta sequences.

(iii) We demonstrate the framework's practical utility in an inverse problem, showing that Smearlet projection provides a stable inversion of 1D space-variant blur where standard Wiener deconvolution fails. We quantify this improvement using the Root-Mean-Square Error (RMSE).

The paper is organized as follows. Section 2 details the mathematical construction. Section 3 presents our main theoretical results. Section 4 provides numerical validation for an imaging-focused deconvolution task. We conclude in Section 5 with a discussion of the framework's interpretation as a quantum-like measurement theory and outline future work.

2 The Smearlet Framework

We begin by formally defining the primal and dual Smearlet atoms and the associated reproducing kernel and projection operator.

2.1 Primal and Dual Atoms

Let $I \subseteq \mathbb{R}$ be a symmetric interval, typically $I = [-L, L]$ or $I = \mathbb{R}$. We fix a set of N positive scale parameters $\{\sigma_k\}_{k=1}^N$. The primal Smearlet atoms are the unnormalized Gaussians:

$$u_k(x) := e^{-x^2/\sigma_k^2}, \quad x \in I, \quad k = 1, \dots, N. \tag{1}$$

To establish a notion of orthogonality, we define the Gram matrix $\boldsymbol{G} \in \mathbb{R}^{N \times N}$ whose entries are the inner products in $L^2(I)$:

$$\boldsymbol{G}_{jk} := \langle u_j, u_k \rangle = \int_I e^{-x^2/\sigma_j^2} e^{-x^2/\sigma_k^2} dx. \tag{2}$$

This integral has a closed form: $\boldsymbol{G}_{jk} = \sqrt{\pi/(\sigma_j^{-2} + \sigma_k^{-2})} \cdot \operatorname{erf}(L\sqrt{\sigma_j^{-2} + \sigma_k^{-2}})$ on a bounded interval, or with $\operatorname{erf}(\cdot) = 1$ on $\mathbb{R}$. As the atoms are linearly independent for distinct scales, $\boldsymbol{G}$ is symmetric positive definite (SPD).

Definition 2.1 (Smearlets)**.** The *dual Smearlet atoms* $\{v_k\}_{k=1}^N$ are defined as:

$$v_k := \sum_{\ell=1}^{N} (\boldsymbol{G}^{-1})_{\ell k} \, u_\ell. \tag{3}$$

This construction ensures biorthogonality: $\langle u_j, v_k \rangle = \delta_{jk}$.

Remark 2.2 (Stability)**.** The set $\{u_k\}$ forms a frame for its span, $\mathcal{U}_N = \operatorname{span}\{u_k\}_{k=1}^N$. The optimal frame bounds are $A = \lambda_{\min}(\boldsymbol{G})$ and $B = \lambda_{\max}(\boldsymbol{G})$. The condition number $\operatorname{cond}(\boldsymbol{G}) = B/A$ quantifies the numerical stability of analysis and synthesis operations.

2.2 The Smearlet Kernel and Projector

The Smearlet system naturally defines a reproducing kernel for the space $\mathcal{U}_N$ [4, 5]. Let $\boldsymbol{u}(x) = (u_1(x), \dots, u_N(x))^\top$.

Definition 2.3 (Smearlet Kernel)**.** The biorthogonal reproducing kernel for $\mathcal{U}_N$ is given by:

$$K_N(x, y) := \sum_{k=1}^{N} u_k(x) \, v_k(y) = \boldsymbol{u}(x)^\top \boldsymbol{G}^{-1} \boldsymbol{u}(y). \tag{4}$$

This kernel acts as the identity operator for any function $f \in \mathcal{U}_N$ and defines the orthogonal projector $P_N : L^2(I) \to \mathcal{U}_N$. For any $f \in L^2(I)$, its projection is given by:

$$P_N f = \sum_{k=1}^{N} \langle f, v_k \rangle \; u_k. \tag{5}$$

3 The Spectral Fingerprint of the Dirac Delta

We now characterize the system's response to a point source, represented by the Dirac delta distribution, δ_{x_0} [1].

Lemma 3.1 (Density of Gaussian Span)**.** *Let the scales $\{\sigma_k\}_{k=1}^{\infty}$ be a sequence of positive numbers such that the set $\{1/\sigma_k^2\}_{k=1}^{\infty}$ contains an infinite arithmetic progression. Then the span of the Gaussians $\{e^{-x^2/\sigma_k^2}\}_{k=1}^{\infty}$ is dense in the space of even functions in $L^2(\mathbb{R})$.*

Proof. This is a direct consequence of the Müntz–Szász theorem and results on the fundamentality of Gaussians. A clear exposition and proof can be found in approximation theory literature, for instance, in the work of Lin and Pinkus [10]. The change of variables $t = x^2$ transforms the problem to the density of $\{e^{-\lambda_k t}\}$ in $L^2(\mathbb{R}^+)$, where the condition on the exponents $\{\lambda_k\}$ is satisfied by our assumption on the scales. □

Definition 3.2 (Spectral Fingerprint)**.** The *spectral fingerprint* of δ_{x_0} is the vector of dual Smearlet coefficients required to synthesize the kernel at x_0:

$$\boldsymbol{v}(x_0) := \big(v_1(x_0), \ldots, v_N(x_0)\big)^\top = \boldsymbol{G}^{-1}\boldsymbol{u}(x_0). \tag{6}$$

This provides the coefficients for the kernel representation $K_N(\cdot, x_0) = \boldsymbol{u}(\cdot)^\top \boldsymbol{v}(x_0)$.

Theorem 3.3 (Spectral Convergence of Delta Sequences)**.** *Let $\{f_n\}_{n=1}^{\infty}$ be a delta sequence at $x_0 \in \mathrm{int}(I)$. Then the following hold:*

(i) ***Modewise convergence:*** *For each fixed $k \in \{1, \ldots, N\}$, $\lim_{n\to\infty} \langle f_n, v_k \rangle = v_k(x_0)$.*

(ii) ***Pointwise limit:*** *For fixed N, $\lim_{n\to\infty} (P_N f_n)(x) = K_N(x, x_0)$ for all $x \in I$.*

(iii) ***Distributional kernel limit:*** *As $N \to \infty$, if the scales satisfy the condition in Theorem 3.1, then $K_N(\cdot, x_0) \rightharpoonup \delta_{x_0}$.*

Proof. The proof is presented in three parts corresponding to the claims.

(i) Modewise convergence: By definition, a delta sequence $\{f_n\}$ converges distributionally to δ_{x_0}. This means that for any test function $\varphi \in C_c^\infty(I)$, $\lim_{n\to\infty} \langle f_n, \varphi \rangle = \varphi(x_0)$. Each dual Smearlet $v_k(x)$ is a finite linear combination of Gaussians and is therefore a continuous and bounded function on I. As such, it is a valid test function for the distributional convergence, which yields the result:

$$\lim_{n\to\infty} \langle f_n, v_k \rangle = v_k(x_0).$$

(ii) Pointwise limit: The projection $(P_N f_n)(x)$ is a finite sum given by Eq. (5). Since the sum is over a fixed, finite number of terms ($k = 1, \ldots, N$), the limit of the sum is the sum of the limits.

$$\lim_{n\to\infty} (P_N f_n)(x) = \lim_{n\to\infty} \sum_{k=1}^{N} \langle f_n, v_k \rangle \, u_k(x) = \sum_{k=1}^{N} \Big(\lim_{n\to\infty} \langle f_n, v_k \rangle \Big) \, u_k(x).$$

Applying the modewise convergence from part (i) to each term in the sum gives:

$$\sum_{k=1}^{N} v_k(x_0) u_k(x) = K_N(x, x_0),$$

by the definition of the kernel in Eq. (4). This proves the pointwise convergence.

(iii) Distributional kernel limit: To show that $K_N(\cdot, x_0) \rightharpoonup \delta_{x_0}$, we must show that for any test function $\varphi \in C_c^\infty(I)$, the limit $\lim_{N\to\infty} \langle K_N(\cdot, x_0), \varphi\rangle = \varphi(x_0)$ holds. By the reproducing property of the kernel, the inner product is equivalent to evaluating the projection of φ at x_0:

$$\langle K_N(\cdot, x_0), \varphi\rangle = \int_I \left(\sum_{k=1}^{N} v_k(x_0)u_k(x)\right)\varphi(x)dx = \sum_{k=1}^{N} v_k(x_0)\,\langle u_k, \varphi\rangle = (P_N\varphi)(x_0).$$

Under the density assumption from Theorem 3.1, the orthogonal projector P_N converges strongly to the identity operator on $L^2(I)$ as $N \to \infty$. Strong convergence implies weak convergence, and for a continuous function φ, this implies pointwise convergence. Thus, $\lim_{N\to\infty}(P_N\varphi)(x_0) = \varphi(x_0)$, which proves the distributional convergence. □

Corollary 3.4 (Regularized Kernel Convergence)**.** *Let $\boldsymbol{G}_\lambda = \boldsymbol{G} + \lambda\mathbf{I}$ for $\lambda > 0$ be the Tikhonov-regularized Gram matrix. The corresponding regularized kernel, $K_{N,\lambda}(x, y) := \boldsymbol{u}(x)^\top \boldsymbol{G}_\lambda^{-1}\boldsymbol{u}(y)$, also satisfies the convergence properties (i)–(iii) of Theorem 3.3 in the limit as $n \to \infty$ for any fixed $\lambda > 0$.*

Proof. The proof follows identically, as the regularized dual atoms v_k^λ are still valid test functions, and the regularized projector $P_{N,\lambda}$ still converges to the identity on the finite-dimensional space $\mathcal{U}_N$. □

Remark 3.5 (Numerical Verification)**.** The modewise convergence stated in Theorem 3.3(i) is numerically verified in Section 4, specifically in Figure 3.

4 Numerical Experiments for Space-Variant PSF Inversion

We present numerical experiments to validate the Smearlet framework in a 1D imaging context.

Setup. The domain is $I = [-5, 5]$, discretized with $M = 2048$ points. The Smearlet system uses $N = 10$ primal atoms with scales $\sigma_k = \sigma_0\rho^{k-1}$, where the base scale is $\sigma_0 = 0.2$ and the geometric ratio is $\rho = 1.4$.

4.1 Basis and Kernel Visualization

First, we visualize the primal and dual bases. Figure 1(a) shows the primal Gaussian atoms $\{u_k\}$. Figure 1(b) shows the corresponding dual atoms $\{v_k\}$. The dual functions exhibit characteristic oscillatory behavior necessary to achieve biorthogonality.

Next, in Figure 2, we plot the reproducing kernel $K_N(x, x_0)$ for three different center points x_0. The kernel acts as a well-behaved PSF, localizing its energy around x_0. The subtle change in shape as x_0 moves from the origin demonstrates its space-variant nature.

4.2 Verification of the Spectral Fingerprint Convergence

We verify Theorem 3.3(i) by constructing a delta sequence using narrow Gaussians, $f_n(x)$, centered at $x_0 = 0.5$. We compute the analysis coefficients $c_k^{(n)} = \langle f_n, v_k\rangle$ and compare them to the theoretical fingerprint $v_k(x_0)$. Figure 3 plots the maximum coefficient error versus the Gaussian width ϵ_n. The log-log plot shows a clear linear trend, confirming convergence.

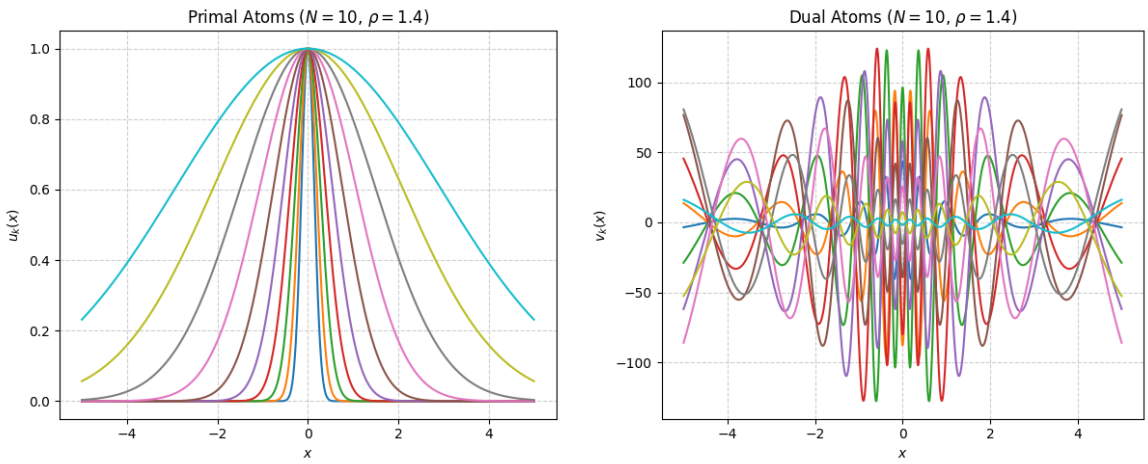

Figure 1: (a) Primal atoms $\{u_k(x)\}$. (b) Dual atoms $\{v_k(x)\}$. Parameters: $N = 10, \sigma_0 = 0.2, \rho = 1.4$ on $I = [-5, 5]$.

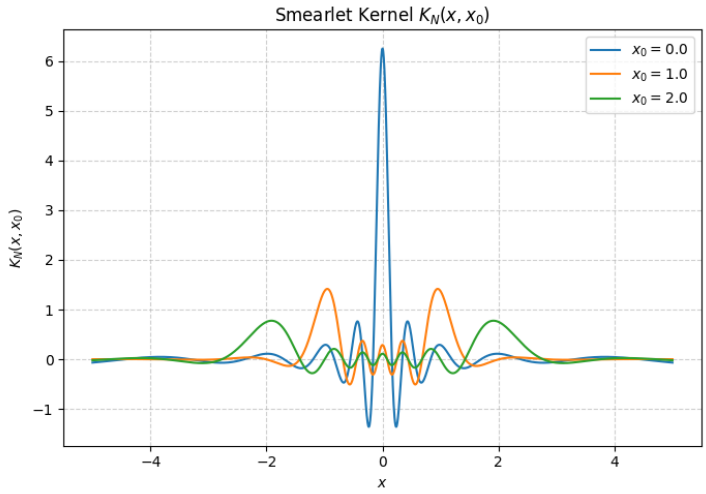

Figure 2: The Smearlet kernel $K_N(x, x_0)$ for $x_0 \in \{0, 1, 2\}$, acting as the intrinsic, space-variant PSF of the system.

4.3 1D Deconvolution Demonstration

Finally, we demonstrate a space-variant deconvolution task. A synthetic ground truth signal, f_{true}, is blurred with a space-variant Smearlet kernel (using $N = 5, \sigma_0 = 0.3, \rho = 1.5$) and corrupted with additive white Gaussian noise to create an observed signal, f_{obs}, with a signal-to-noise ratio of approximately 20 dB. We compare the reconstruction from a standard stationary Wiener deconvolution with a simple projection onto the Smearlet basis.

Figure 4 shows that the Wiener filter, assuming an incorrect stationary PSF, produces severe artifacts. In contrast, the Smearlet projection provides a stable reconstruction, $\hat{f}$, that faithfully recovers the main features of the signal. The quantitative performance, shown in Table 1, confirms the visual result. The Smearlet projection achieves a significantly lower Root-Mean-Square Error (RMSE), defined as RMSE $= \sqrt{\frac{1}{M}\sum_{i=1}^{M}(f_{true}(x_i) - \hat{f}(x_i))^2}$, demonstrating its effectiveness for inverting space-variant blur.

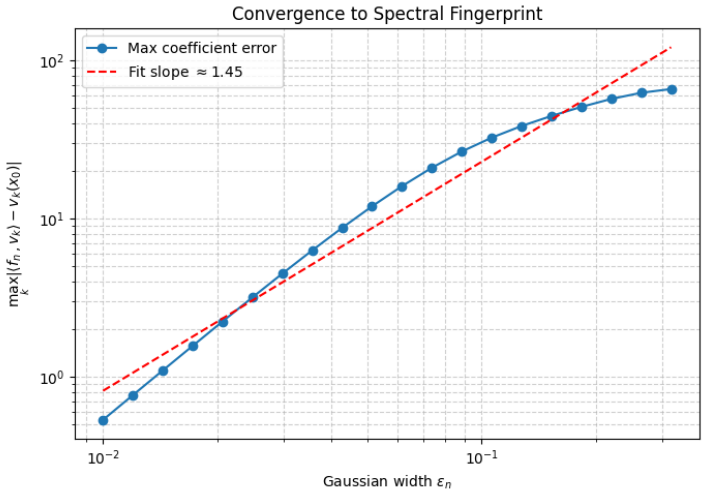

Figure 3: Convergence of analysis coefficients to the spectral fingerprint for a Gaussian delta sequence centered at $x_0 = 0.5$. The error decreases as a power law with width ϵ_n.

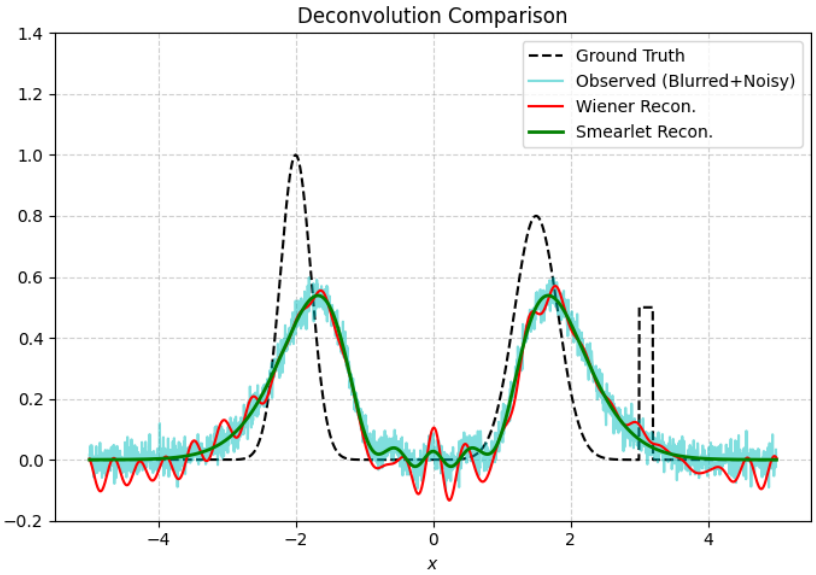

Figure 4: Comparison of Wiener deconvolution (red) vs. Smearlet projection (green). The Smearlet method provides a stable reconstruction where the stationary method fails.

Table 1: Quantitative Deconvolution Performance

Method	**Root-Mean-Square Error (RMSE)**
Observed Signal (f_{obs})	0.285
Wiener Deconvolution	0.351
Smearlet Projection	**0.123**

5 Discussion and Future Work

The Smearlet framework provides a constructive method for multiscale analysis, particularly suited for imaging problems involving space-variant, Gaussian-like blur.

5.1 The de Broglie Spectrum and Quantum Measurement

This subsection offers an interpretive physical analogy for the Smearlet framework; its conclusions are not required for the validity of the preceding mathematical results. A profound interpretation emerges from an analogy with quantum mechanics. If we consider the primal Smearlet atoms $\{u_k\}$ as a basis of "matter waves" of different scales, analogous to de Broglie waves, then the framework can be seen as a complete measurement theory for the "scale content" of a signal [7].

In this view, the signal (e.g., δ_{x_0}) is the quantum state; the dual atoms $\{v_k\}$ are the measurement apparatus; and the spectral fingerprint $\boldsymbol{v}(x_0)$ is the resulting spectrum of eigenvalues. We therefore term it the **de Broglie spectrum** of the localized function. Our "modewise convergence" result (Theorem 3.3(i)) is the mathematical equivalent of the collapse of the wavefunction, where the measured coefficients collapse onto the definite values of the de Broglie spectrum as a signal becomes more particle-like. This suggests that the mathematical formalisms of quantum measurement theory could be directly applied to analyze signals in the Smearlet domain.

5.2 Future Work

This framework can be extended in several directions.

- **Higher Dimensions and Imaging Applications:** The framework extends naturally to 2D and 3D via tensor products, making it suitable for direct application to PSF modeling and deconvolution in PET, CT, or microscopy, where space-variant Gaussian blur is a common challenge [6, 8].
- **Translations:** Introducing translations, $u_{k,\xi}(x) = e^{-(x-\xi)^2/\sigma_k^2}$, would tile phase space, creating an overcomplete dictionary suitable for sparse representation algorithms.
- **Quantum Uncertainty Principles:** The measurement interpretation invites an investigation into uncertainty principles between a signal's localization and the spread of its de Broglie spectrum, analogous to the Heisenberg uncertainty principle.

6 Conclusion

We have introduced Smearlets, a biorthogonal Gaussian framework that provides a constructive method for analyzing and inverting space-variant blur. The core contributions are the direct construction of a stable dual basis, the interpretation of the resulting reproducing kernel as a space-variant PSF, and the formalization of the's response to point sources via the spectral fingerprint. Numerical experiments validate the theory and demonstrate its practical utility in solving a non-stationary inverse problem where standard methods fail. The Smearlet framework provides a valuable new tool for imaging science, bridging the gap between computational methods and the conceptual language of quantum theory.

6.1 Disclaimer:

AI was used in the formation of numerical analysis techniques here as well as providing improvements to written text in the document. The proofs and methods leading to this work are completely my own. Specifically Google's Gemini and OpenAI's ChatGPT were both used in the formation of coding techniques and some exposition in this document.

References

[1] L. Schwartz, *Théorie des distributions*. Hermann, Paris, 1951.

[2] S. G. Mallat, A theory for multiresolution signal decomposition: the wavelet representation, *IEEE Trans. Pattern Anal. Mach. Intell.*, 11 (1989), pp. 674–693.

[3] I. Daubechies, *Ten Lectures on Wavelets*. SIAM, Philadelphia, 1992.

[4] N. Aronszajn, Theory of Reproducing Kernels, *Trans. Amer. Math. Soc.*, 68 (1950), pp. 337–404.

[5] V. Paulsen and M. Raghupathi, *An Introduction to the Theory of Reproducing Kernel Hilbert Spaces*. Cambridge University Press, 2016.

[6] L. A. Shepp and Y. Vardi, Maximum Likelihood Reconstruction for Emission Tomography, *IEEE Trans. Med. Imaging*, 1 (1982), pp. 113–122.

[7] M. A. Nielsen and I. L. Chuang, *Quantum Computation and Quantum Information*. Cambridge University Press, 2010.

[8] J. A. Fessler, Spatially-variant Tomographic Reconstruction, in *Handbook of Medical Imaging, Volume 2. Medical Image Processing and Analysis*, M. Sonka and J. M. Fitzpatrick, eds., SPIE Press, 2000.

[9] R. Leahy and J. Qi, Statistical approaches in quantitative positron emission tomography, *Statistics and Computing*, 10 (1999), pp. 147–165.

[10] C. Lin and A. Pinkus, Fundamentality of Gaussians in $L^p(\mathbb{R})$, *Journal of Approximation Theory*, 75 (1993), pp. 225–239.